ELSEVIER

www.elsevier.nl/locate/jorganchem

Journal of Organometallic Chemistry 591 (1999) 194–203

Journal of Organometallic Chemistry

$(Silox)_3Nb(\eta^2\text{-N,C-4-picoline})$ as a source of $(silox)_3Nb$: structure of $[(silox)_3Nb]_2(\mu\text{-}\eta^2,\eta^2\text{-}C_6H_6)$ (silox = ^{t}Bu$_3$SiO)

Adam S. Veige, Troy S. Kleckley, Rebecca M. Chamberlin, David R. Neithamer, Christina E. Lee, Peter T. Wolczanski *, Emil B. Lobkovsky, Wingfied V. Glassey

Department of Chemistry and Chemical Biology, Cornell University, Baker Laboratory, Ithaca, NY 14853, USA

Received 23 June 1999; accepted 9 September 1999

Abstract

Electrochemical and chemical reductions of $(silox)_3NbCl_2$ (**1**, −1.42 V versus Ag/Ag^+) and $(silox)_3TaCl_2$ (**2**, −2.18 V) generated $[(silox)_3NbCl_2]^-$ ($\mathbf{1}^-$) and $[(silox)_3TaCl_2]^-$ ($\mathbf{2}^-$). The anions were subject to Cl^- loss, leading to $(silox)_3NbCl$ (**3**) and probable disproportionation (Ta). Complex **3** formed reversible solvent adducts $(silox)_3ClNbL$ (**3**-L, L = THF, py). Na/Hg reduction of $(silox)_3NbCl_2$ (**1**) in the presence of 4-picoline afforded $(silox)_3Nb(\eta^2\text{-N,C-4-NC}_5H_4CH_3)$ (**6**), which can be considered a source of '$(silox)_3Nb$', analagous to $(silox)_3Ta$ (**4**). Adducts such as $(silox)_3Nb(\eta^2\text{-H}_2CCHR)$ (R = H, **7**; Ph, **8**) may be formed upon addition of olefins, and **6** abstracted an oxygen from N_2O, NO or ethylene oxide to give $(silox)_3Nb{=}O$ (**9**) and N_2 or C_2H_4, respectively, which are reactions also observed for **4**. 4-Picoline may be abstracted from **6** by **4** to give $\{(silox)_3Nb\}_2(\mu{:}\eta^2,\eta^2\text{-}C_6H_6)$ (**11**) and $(silox)_3Ta(\eta^2\text{-N,C-4-NC}_5H_4CH_3)$ (**12**). An X-ray structure determination of **11** revealed a disordered bridge that was modeled as a $\mu{:}\eta^2,\eta^2$-benzene. Extended Hückel molecular orbital (EHMO) calculations showed that the $\mu{:}\eta^2,\eta^2$-configuration was energetically better than a $\mu{:}\eta^6,\eta^6$-alternative, but about the same as a plausible $\mu{:}\eta^3,\eta^3$-arrangement.

Keywords: Niobium; Tantalum; Picoline; Benzene; Reduction; Atom abstraction

1. Introduction

The resurgence in the chemistry of three-coordination stems in part from dramatic small molecule activations exhibited by early transition metal complexes containing hard, electronegative ligands [1]. Highlights include the scission of dinitrogen by $Mo\{N(^t\text{Bu})Ar\}_3$ (Ar = Ph, 3,5-$C_6H_3Me_2$, 4-C_6H_4F) to afford $\{Ar(^t\text{Bu})N\}_3Mo{\equiv}N$ [2], and the related (R = 3,5-$C_6H_3Me_2$) activation of N_2O to yield $\{Ar(^t\text{Bu})N\}_3Mo{\equiv}N$ and $\{Ar(^t\text{Bu})N\}_3Mo(NO)$, a reaction that features a thermodynamically improbable N–N bond cleavage [3]. NO deoxygenation was also achieved by employing the organometallic reagent $(Mes)_3V(THF)$ [4], a plausible source of $(Mes)_3V$, to attack $\{Ar(R)N\}_3Cr(NO)$ (R = $C(CD_3)_2CH_3$, Ar = 3,5-$C_6H_3Me_2$, 2,5-C_6H_3FMe), producing $\{Ar(R)N\}_3Cr{\equiv}N$ and $(Mes)_3V{=}O$. A similar deoxygenation of styrene-oxide by the vanadium complex has also been observed [5]. In contrast to these substrate-induced, multielectron metal oxidations, a variety of dinuclear, 1 e^- oxidative addition reactions with X_3Ti (X = amide [1], aryloxide [6], siloxide) [7] have also been reported. An unusual ring-opening of THF by $(silox)_3Ti$ (silox = ^{t}Bu$_3$SiO) to yield $(silox)_3TiOCH_2(CH_2)_2CH_2Ti(silox)_3$ [7], the reversible coupling of benzophenone to give $(silox)_3TiOC(Ph)_2\text{-}(C(H)C_4H_4C){=}C(Ph)OTi(silox)_3$, and related titanium–ketyl chemistry are contributions from these laboratories [8].

Unlike transformations that require formal oxidation state changes, carbon–hydrogen bond activations by transient, three-coordinate imido complexes are predominantly electrophilic reactions mediated by d^0 metal centers. 1,2-RH-addition to $X_{3-n}M(=NSi^t\text{Bu}_3)_n$ (X = $HNSi^t\text{Bu}_3$, M = Ti, $n = 1$ [9]; M = Zr, Hf, $n = 1$ [10]; M = V [11], Ta [12], $n = 2$; M = W [13], $n = 3$; X = $OSi^t\text{Bu}_3$, M = Ti, $n = 1$) [14] is the likely mechanism for formation of $X_{3-n}(^t\text{Bu}_3SiNH)M(=NSi^t\text{Bu}_3)_{n-1}(R)$. The last system provided a thorough, general overview of

* Corresponding author. Fax: +1-607-255-4137.
E-mail address: ptw2@cornell.edu (P.T. Wolczanski)

0022-328X/99/$ - see front matter
PII: S0022-328X(99)00524-0

the energetics and selectivity in C–H bond activation.

In these laboratories [15], considerable effort has been focused on delineating the reactions of $(silox)_3Ta$, a rare, low-valent, trigonal complex with a tremendous capability for various bond activations. As Scheme 1 illustrates, CO cleavage occurs at $\sim 5°C$ to afford the dicarbide $[(silox)_3Ta]_2(\mu{:}\eta^1,\eta^1\text{-}C_2)$ and oxo $(silox)_3Ta{=}O$ [16], a reaction relevant to the dissociative adsorption of CO in the Fischer–Tropsch process. EH activation of $PhEH_2$ (E = N, P, As) provided $(silox)_3HTaEHPh$, whose subsequent 1,2-H_2 eliminations led to the formation of $(silox)_3Ta{=}EPh$ derivatives [17]. Accompanying this chemistry was the unexpected observation of *p*-X-aniline C–N bond oxidative addition when X is sufficiently electron withdrawing (e.g. $X = CF_3$) [18].

Given the interesting chemistry associated with $(silox)_3Ta$, the niobium analogue was sought. While an η^2-N,C-pyridine derivative analogous to $(silox)_3Ta(\eta^2$-N,C-py) [19,20] was synthesized, the niobium complex proved to be far more reactive, losing 0.5 equivalents of py and ring-opening pyridine to various isomers of $(silox)_3Nb{=}CHCH{=}CHCH{=}CHN{=}Nb(silox)_3$ [21,22]. The reaction may occur through the generation of '$(silox)_3Nb$' and its subsequent attack of $(silox)_3Nb(\eta^2$-N,C-py), and represents a different py cleavage pathway than previously observed [23]. The pursuit of $(silox)_3Nb$ is certainly warranted on this basis, and herein a masked version is reported.

2. Results and discussion

2.1. Direct reductions of $(silox)_3NbCl_2$ (1)

Early attempts to generate '$(silox)_3Nb$' centered on reductions of $(silox)_3NbCl_2$ (**1**) that paralleled those of $(silox)_3TaCl_2$ (**2**) [16]. Electrochemical studies indicated that the M(V)/M(IV) reduction was substantially less negative for Nb. As Eq. (1) indicates, a reversible wave corresponding to the reduction of **1** to $[(silox)_3NbCl_2]^-$ ($\mathbf{1}^-$) was observed at -1.42 V (versus Ag/Ag^+; -1.14 V versus NHE), and a similar, reversible reduction of **2** to $[(silox)_3TaCl_2]^-$ ($\mathbf{2}^-$) was seen at -2.18 V (versus Ag/Ag^+; -1.90 V versus NHE). Further reductions of $\mathbf{1}^-$ and $\mathbf{2}^-$ were not observed prior to solvent reduction (< -3.0 V).

$$\underset{M = Nb,\ \mathbf{1};\ Ta,\ \mathbf{2}}{(silox)_3MCl_2} \overset{THF,\ E^\circ_{red}}{\underset{E^\circ_{ox}}{\rightleftharpoons}} \underset{M = Nb,\ \mathbf{1}^-;\ Ta,\ \mathbf{2}^-}{[(silox)_3MCl_2]^-} \quad (1)$$

$$\underset{M = Nb,\ \mathbf{1};\ Ta,\ \mathbf{2}}{(silox)_3MCl_2} + [^nBu_4N]Cl \xrightarrow[THF]{Na/Hg} \underset{M = Nb,\ [^nBu_4N]\ \mathbf{1};\ Ta,\ [^nBu_4N]\ \mathbf{2}}{[^nBu_4N][(silox)_3MCl_2]} \quad (2)$$

Corroboration of anion formation was obtained via direct synthesis. Reduction of $(silox)_3MCl_2$ (M = Nb, **1**; Ta, **2**, Eq. (2)) in the presence of $[^nBu_4N]Cl$ afforded salts tentatively formulated as $[^nBu_4N][(silox)_3NbCl_2]$ ($[^nBu_4N]\mathbf{1}$) and $[^nBu_4N][(silox)_3TaCl_2]$ ($[^nBu_4N]\mathbf{2}$). While the latter was isolated as turquoise crystals in 81% yield, the similarly colored niobium derivative was pre-

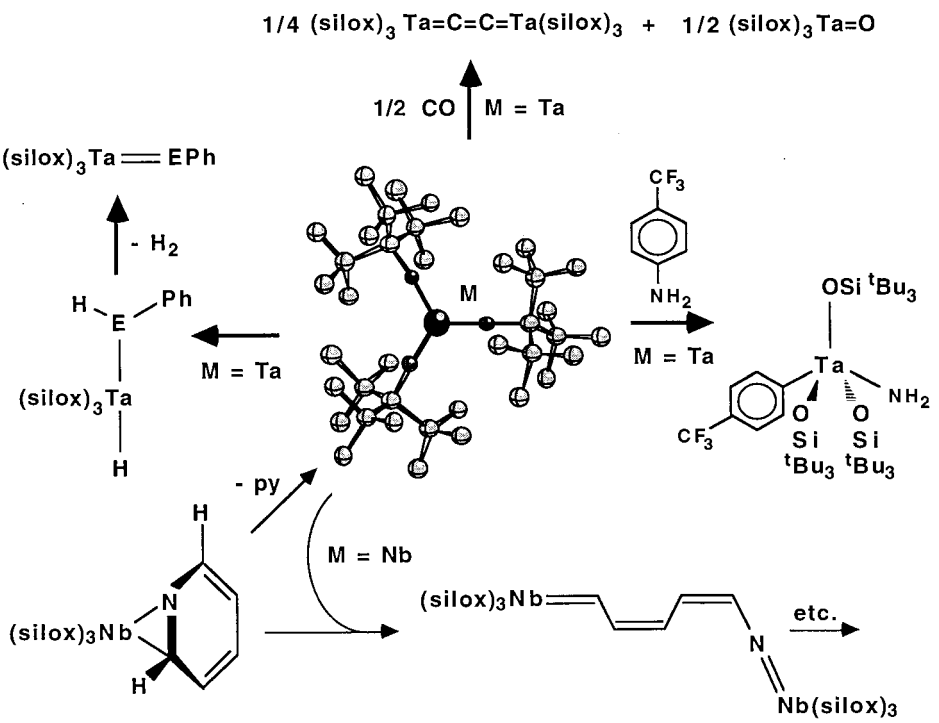

Scheme 1.

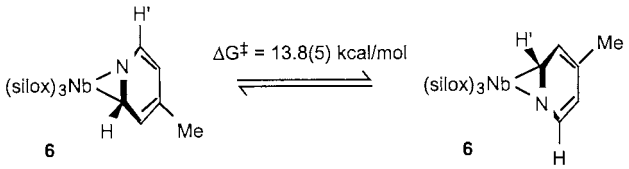

Fig. 1.

cipitated as a powder, and attempts to spectroscopically characterize the paramagnetic compounds by ^{1}H-NMR revealed impurities due to Cl^- loss and related decomposition. UV–vis spectra were consistent with trigonal bipyramidal structures ([^{n}Bu$_4$N]**1**: $\lambda = 652$ nm, $\varepsilon = 79$ M^{-1} cm^{-1}; $\lambda \sim 460$ nm (sh), $\varepsilon = 40$ M^{-1} cm^{-1}. [^{n}Bu$_4$N]**2**: $\lambda = 648$ nm, $\varepsilon = 85$ M^{-1} cm^{-1}; $\lambda \sim 450$ nm (sh), $\varepsilon = 30$ M^{-1} cm^{-1}) [24], but no further attempts at characterization were made.

Since the niobium dichloride anion (**1**$^-$) appeared to degrade, sequential reduction attempts toward '(silox)$_3$Nb' were explored. Treatment of (silox)$_3$NbCl$_2$ (**1**) with a slight excess of Na as its amalgam afforded a turquoise solution containing, presumably, [Na(THF)$_x$][(silox)$_3$NbCl$_2$] ([Na(THF)$_x$]**1**, Eq. (3)). Upon isolation, Na(THF)$_x$**1** quickly lost crystallinity and discolored, fading first to pale green, then to a grayish purple powder upon exposure to vacuum. Residual THF was removed upon trituration with hexanes, and (silox)$_3$NbCl (**3**, Eq. (4)) was isolated as purple crystals in 76% overall yield.

$$\underset{\mathbf{1}}{(silox)_3NbCl_2} \xrightarrow[1\ h]{Na/Hg,\ THF} \underset{[Na(THF)_x]\mathbf{1}}{[Na(THF)_x][(silox)_3NbCl_2]} \quad (3)$$

$$[Na(THF)_x]\mathbf{1} \xrightarrow[-NaCl,\ -x\ THF]{hexanes} \underset{\mathbf{3}}{(silox)_3NbCl} \quad (4)$$

No epr signal was detected at -78°C, and an Evans method measurement revealed a magnetic moment of 1.65 μ_B (C_6D_6), consistent with a d^1 pseudo-T_d molecule with the electron residing in the degenerate d_{xz}, d_{yz} orbital set. A molecular weight measurement was consistent with a monomeric formulation (found 754; calc. 775), while cyclic voltammetry experiments were precluded due to the reaction of **3** with various electrolytes.

The analogous tantalum(IV) derivative could not be isolated from the related reduction, although a turquoise color attributed to [Na(THF)$_x$][(silox)$_3$TaCl$_2$] (Na(THF)$_x$**2**) can be observed. Only (silox)$_3$Ta (**4**) and the starting dichloride (**2**) can be observed upon work-up of the reaction. It is plausible that (silox)$_3$TaCl is generated upon Cl^- loss Na(THF)$_x$**2**, and subsequent disproportionation to **2** and (silox)$_3$Ta ensues. While ^{1}H-NMR spectra of [^{n}Bu$_4$N][(silox)$_3$TaCl$_2$] ([^{n}Bu$_4$N]**2**) suggest that disproportion does occur, it is still possible that (silox)$_3$TaCl is more susceptible to reduction than (silox)$_3$TaCl$_2$ (**2**).

In the presence of donors, (silox)$_3$NbCl (**3**) provided evidence of adduct formation. THF solutions of **3** at -78°C were blue–green, hinting at the presence of (silox)$_3$ClNb(THF) (**3**-THF), while the purple color attributed to the unsolvated complex characterized solutions at 25°C (Eq. (5)). Use of the stronger donor pyridine permitted isolation of (silox)$_3$ClNb(py) as a blue powder from an ink-blue solution according to Eq. (6). Characteristic paramagnetically shifted py resonances were in accord with an η^1-bound py ligand, and ^{1}H-NMR spectra indicated trace equilibrium amounts of **3**.

$$\underset{\mathbf{3}}{(silox)_3NbCl} \overset{THF}{\rightleftharpoons} \underset{\mathbf{3}\text{-THF}}{(silox)_3ClNb(THF)} \quad (5)$$

$$\mathbf{3} \overset{pyridine}{\rightleftharpoons} \underset{\mathbf{3}\text{-py}}{(silox)_3ClNb(py)} \quad (6)$$

2.2. Synthesis of (silox)$_3$Nb(η^2-N,C-4-NC$_5$H$_4$CH$_3$) (6)

In a fashion similar to the synthesis of (silox)$_3$Nb(η^2-N,C-py) (**5**) [21], reduction of (silox)$_3$NbCl$_2$ (**1**) with 2.1 equivalents of Na/Hg in Et$_2$O containing ~ 30 equivalents 4-picoline, afforded brown (silox)$_3$Nb(η^2-N,C-4-NC$_5$H$_4$CH$_3$) (**6**) in 42% yield upon crystallization from hexanes (Eq. (7)). Unlike the pyridine and the 2- and 3-picoline adducts [21,22], **6** does not readily ring open to an alkylidene–imide dinuclear complex. Four distinct proton resonances corresponding to the η^2-4-picoline ligand were observed at -50°C in toluene-d_8, and a fluxional process that equilibrates *o*- and *m*-4-picoline hydrogens was observed at higher temperatures.

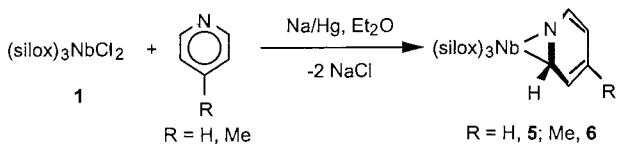

(7)

Coalescence of the *m*-protons occurred at 40°C, corresponding to an oscillation between the two η^2-N,C binding sites of **6** that has a barrier of $\Delta G^{\ddagger} = 13.8(5)$ kcal mol^{-1}, as illustrated in Fig. 1.

Since 4-picoline ring opening is sluggish, (silox)$_3$Nb(η^2-N,C-4-NC$_5$H$_4$CH$_3$) (**6**) may be considered a precursor to '(silox)$_3$Nb'. Some simple reactions were conducted to support this contention. First, both (silox)$_3$Nb(η^2-N,C-py) (**5**) and **6** can be substituted by ethylene and styrene to provide (silox)$_3$Nb(η^2-H$_2$CCHR) (R = H, **7**; Ph, **8**), as indicated by Eq. (8). Ethylene adduct **7** was prepared on a NMR tube scale in C_6D_6 in quantitative yield (C_6D_6, < 5 m, 25°C), while the styrene adduct was isolated as green–brown crystals in 44% yield from pentanes.

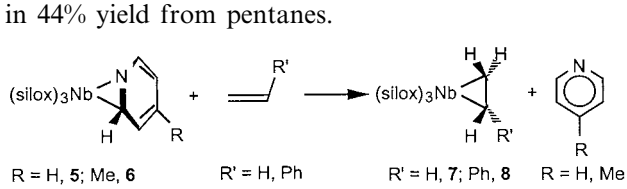

(8)

They are illustrated as metallacyclopropanes in reference to the highly reduced nature of the Nb(III) metal center; the styrene H–H coupling constants are consistent with this interpretation.

2.3. Atom abstractions by '(silox)$_3$Nb'

The atom abstraction capability of (silox)$_3$Nb(η^2-N,C-4-NC$_5$H$_4$CH$_3$) (**6**) was tested in comparison to the aforementioned reactions. Treatment of **6** with an excess of N_2O in benzene afforded (silox)$_3$Nb=O (**9**) as an off-white powder in 53% yield (Eq. (9)).

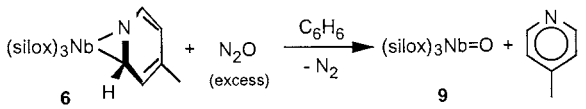

(9)

The niobium–oxo stretch was tentatively assigned to a medium strength band at 884 cm^{-1} (Nujol) in comparison with the related oxo stretch of (silox)$_3$Ta=O observed at 905 cm^{-1} [16]. According to the convention proposed by Bercaw [25], **9** is classifed as — or approaching — a class b oxo, i.e. one considered to have a single strong π-bond. ^{1}H-NMR monitoring of an NMR tube scale reaction indicated quantitative conversion to **9** and free 4-picoline.

Deoxygenation of NO was also effected by (silox)$_3$Nb(η^2-N,C-4-NC$_5$H$_4$CH$_3$) (**6**). Exposure of **6** to an excess of NO immediately yielded oxo (silox)$_3$Nb=O (**9**), 4-picoline, and, presumably, 0.5 equivalents of N_2 according to ^{1}H-NMR (C_6D_6) monitoring (Eq. (10)).

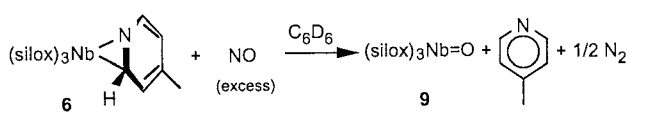

(10)

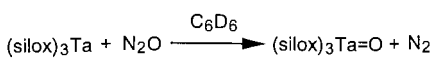

(11)

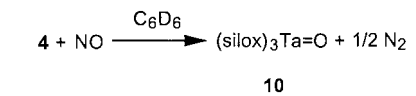

(12)

These bond cleavages were reminescent of related N–O bond breaking events observed when (silox)$_3$Ta (**4**) was exposed to N_2O (Eq. (11)) or NO (Eq. (12)). Clean conversions to oxo (silox)$_3$Ta=O (**10**), and presumably N_2, were noted in both cases, lending credence to the suggestion that **6** is an able source of '(silox)$_3$Nb'.

When 1.1 equivalents of ethylene oxide were admitted to an NMR tube containing (silox)$_3$Nb(η^2-N,C-4-NC$_5$H$_4$CH$_3$) (**6**), the slow (3 d, 25°C) conversion to a $\sim$1.5:1 mixture of oxo (silox)$_3$Nb=O (**9**) and ethylene adduct (silox)$_3$Nb(η^2-C$_2$H$_4$) (**7**) was noted (Eq. (13)).

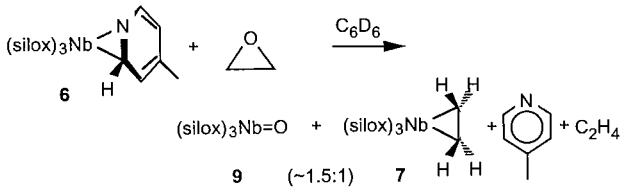

(13)

This contrasts with the swift deoxygenation of ethylene oxide (25°C, immediate) observed for (silox)$_3$Ta (**4**), which produced a similar mixture of products, (silox)$_3$Ta=O (**10**) and (silox)$_3$Ta(η^2-C$_2$H$_4$), when a stoichiometric amount of substrate was used [18]. The difference in rates of reaction is undoubtedly due to the need to lose 4-picoline — either dissociatively or associatively — prior to or concurrent with deoxygenation.

2.4. 4-Picoline abstraction

The affinity for binding picolines is greater for tantalum than for niobium. As a consequence, if 4-picoline dissociation from (silox)$_3$Nb(η^2-N,C-4-NC$_5$H$_4$CH$_3$) (**6**) can be assumed, (silox)$_3$Ta (**4**) can compete for the ligand, yielding free '(silox)$_3$Nb'. Treatment of **6** with 1.1 equivalents of **4** in C_6H_6 gave a brown solution initially, but after 2 h a purple–red precipitate formed (**11**), and soluble (silox)$_3$Ta(η^2-N,C-4-NC$_5$H$_4$CH$_3$) (**12**) [20] was identified by ^{1}H-NMR spectroscopy (Eq. (14)). X-ray structure determination of the virtually insoluble material identified the microcrystalline compound as {(silox)$_3$Nb}$_2$(μ:η^2,η^2-C$_6$H$_6$) (**11**).

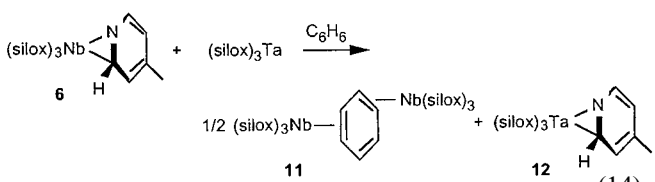

(14)

NMR spectroscopic analysis proved fruitless because of the low solubility of **11**, but IR (Nujol) spectroscopy revealed 889, 834 and 811 cm^{-1} bands that correspond to those exhibited by {(silox)$_3$Ta}$_2$(μ-C$_6$H$_6$) [19], whose solubility was similarly limited [20]. Attempts to generate '(silox)$_3$Nb' from related procedures in non-binding solvents have thus far escaped interpretation.

2.5. Structure of {(silox)$_3$Nb}$_2$(μ:η^2,η^2-C$_6$H$_6$) (11)

A single crystal of {(silox)$_3$Nb}$_2$-(μ:η^2,η^2-C$_6$H$_6$) (**11**) that was isolated from the reaction medium proved amenable to X-ray diffraction studies. The binuclear compound crystallized in space group $P\bar{1}$ (triclinic, Table 1) and while data collection was routine, structure refinement revealed a disorder in the bridging benzene, which resides on an inversion center. A disorder model with two benzenes at half occupancy in μ:η^2,η^2-bonding geometries proved to be best, but in

Table 1
X-ray structural data for $\{(silox)_3Nb\}_2(\mu{:}\eta^2,\eta^2\text{-}C_6H_6)$ (**11**)

Formula	$C_{45}H_{90}O_3Si_3Nb$
Formula weight	856.38
Crystal system	Triclinic
Space group	$P\bar{1}$
λ (Mo–K_α)	0.71073
a (Å)	12.6179(3)
b (Å)	13.2658(3)
c (Å)	16.6123(4)
α (°)	83.6145(11)
β (°)	77.4877(3)
γ (°)	64.0718(2)
V (Å^3)	2440.96(10)
T (K)	173(2)
Z	2
$\rho_{calc.}$ (g cm^{-3})	1.165
μ (mm^{-1})	0.355
Reflections	14034
Independent reflections	10041 ($R_{int} = 0.0354$)
R_1 [$I > 2\sigma(I)$] [a]	0.0666
wR_2 [$I > 2\sigma(I)$] [b]	0.1649
R_1 (all data) [a]	0.0935
wR_2 (all data) [b]	0.1869
GOF on F^2 [c]	1.162

[a] $R_1 = \Sigma\|F_o| - |F_c\|/\Sigma|F_o|$.
[b] $wR_2 = [\Sigma w(|F_o| - |F_c|)^2/\Sigma wF_o^2]^{1/2}$.
[c] GOF $= [\Sigma w(|F_o| - |F_c|)^2/(n-p)]^{1/2}$, n = number of independent reflections, p = number of parameters.

order to obtain realistic parameters, restraints on the bridging group were required (Table 2). The resulting distorted $\mu{:}\eta^2,\eta^2$-bonding configuration [26,27] (Fig. 2) is very similar to that generated for $\{(silox)_3Ta\}_2(\mu\text{-}C_6H_6)$, in which a related disorder model was used [19].

The remainder of the structure was normal, with the two $(silox)_3Nb$ centers in a pseudo-D_{3d} arrangement. The niobium–oxygen bond distances are typical (1.925(14) Å (ave)), while two of the O–Nb–O angles are greater (113.04(11)°, 113.41(11)°), and one less (105.65(11)°) than expected for a pseudo-T_d metal center. The silox ligands are bound to the niobium in a nearly linear (169.8(35)°) fashion, as expected [15]. Two carbons on each half-occupied benzene are within standard bonding distance (2.148(8), 2.276(8) Å; 2.189(7), 2.265(8) Å), but some asymmetry in the η^2-bonding is apparent, as a third niobium–carbon distance is only 2.742(8) Å (3.004(8) Å). Since the disorder of the bridge obfuscates the true nature of the bonding, and significant deviations from reasonable geometric parameters are still apparent even in the best model, interpretation of the $\mu{:}\eta^2,\eta^2$-benzene features should be done with caution.

2.6. EHMO conformational study of $\{(silox)_3Nb\}_2(\mu\text{-}C_6H_6)$ (11)

In crystallographic investigations of $\{(silox)_3Nb\}_2(\mu{:}\eta^2,\eta^2\text{-}C_6H_6)$ (**11**) and $\{(silox)_3Ta\}_2(\mu{:}\eta^2,\eta^2\text{-}C_6H_6)$, disorder models portrayed the bridge as a $\mu{:}\eta^2,\eta^2$-benzene distorted slightly toward a $\mu{:}\eta^3,\eta^3$-configuration. The ambiguity in the crystallographic model prompted an extended Hückel molecular orbital (EHMO) investigation of this interesting bridge. Three distinct (i.e. undistorted) bonding modes were examined within an appropriate model complex, $\{(HO)_3Nb\}_2(\mu\text{-}C_6H_6)$ (**11′**): $\mu{:}\eta^6,\eta^6$-(**11′**-6,6), $\mu{:}\eta^3,\eta^3$-(**11′**-3,3) and $\mu{:}\eta^2,\eta^2$-configurations (**11′**-2,2).

A significant number of EHMO studies have adequately addressed the pyramidal X_3M fragment and its interactions with various ligands [20]. In order to use a

Table 2
Interatomic distances (Å) and angles (°) pertaining to $[(silox)_3Nb]_2(\mu\text{-}\eta^2,\eta^2\text{-}C_6H_6)$ (**11**) [a]

Interatomic distances					
Nb–O1	1.925(2)	Nb–C1	2.742(8)	C1–C2	1.412(11)
Nb–O2	1.912(2)	Nb–C2	2.148(8)	C2–C3	1.458(10)
Nb–O3	1.939(2)	Nb–C3	2.276(8)	C1–C3AA	1.426(10)
O1–Si1	1.678(3)	Nb–C3A	3.004(8)	C1A–C2A	1.468(11)
O2–Si2	1.668(3)	Nb–C2A	2.189(7)	C2A–C3A	1.448(11)
O3–Si3	1.665(3)	Nb–C1A	2.265(8)	C3–C1AA	1.496(10)
SiC–C_{ave}	1.539(10)	Si–C_{ave}	1.926(9)		
Interatomic angles					
O1–Nb–O2	113.04(11)	O1–Nb–O3	105.62(11)	O2–Nb–O3	113.41(11)
Nb–O1–Si1	169.6(2)	Nb–O2–Si2	166.4(2)	Nb–O3–Si3	173.3(2)
O1–Nb–C2	105.6(3)	O2–Nb–C2	123.2(3)	O2–Nb–C3	94.5(3)
O1–Nb–C3	98.8(2)	O3–Nb–C2	93.2(3)	O3–Nb–C3	130.6(2)
O1–Nb–C2A	89.2(2)	O2–Nb–C2A	115.3(3)	O3–Nb–C2A	117.2(3)
O1–Nb–C1A	125.5(3)	O2–Nb–C1A	105.2(2)	O3–Nb–C1A	92.4(2)
C1–C2–C3	117.1(9)	C2–C1–C3AA	122.5(7)	C2–C3–C1AA	118.5(7)
C1A–C2A–C3A	117.0(8)	C2A–C1A–C3B	118.3(7)	C2A–C3A–C1B	121.5(7)
Si–C–C_{ave}	111.8(16)	C–C(Si)–C_{ave}	107.0(13)		

[a] The $\mu\text{-}\eta^2,\eta^2\text{-}C_6H_6$ bridge is modeled by two rings at half-occupancy and restrained (d(CC) = 1.40, planar benzene); its distances and angles should not be considered accurate. Furthermore, all distances and angles associated with the modeled benzene carbons should be viewed as approximate.

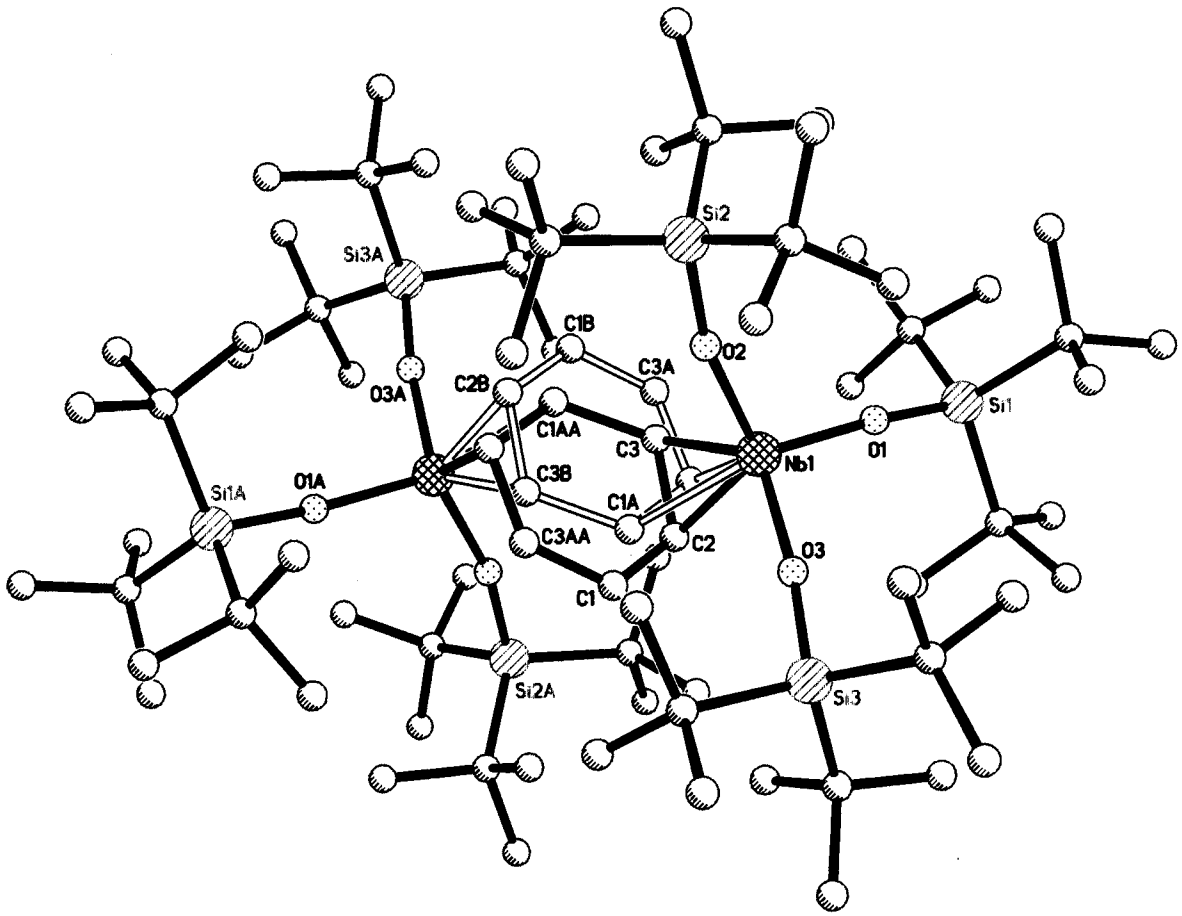

Fig. 2. Molecular view of $\{(silox)_3Nb\}_2(\mu{:}\eta^2,\eta^2\text{-}C_6H_6)$ (**11**) showing the two half-occupancy, $\mu{:}\eta^2,\eta^2$-benzene bridges.

different approach to this particular problem, **11′** was first partitioned into two fragments, the benzene and $(HO)_3Nb\cdots Nb(OH)_3$ components. The interfragment interaction energy was calculated for the linear transits **11′**-6,6 → **11′** − 3,3 and **11′** − 6,6 → **11′**-2,2 as defined by varying the lengths d_1 and d_2 illustrated in Fig. 3 [28]. The $(HO)_3Nb$ fragments were constructed with C_3 symmetry and closely resemble the NbO_3 core of the $(silox)_3Nb$ moieties found in the crystal structure of **11**: $d(Nb\text{–}O) = 1.92$ Å, $d(O\text{–}H) = 0.96$ Å; ∠O–Nb–O = 110.9°, ∠H–O–Nb = 169.6°. The benzene ring was constructed using C–C and C–H bond lengths of 1.399 and 1.101 Å, respectively [29]. The Nb-ring centroid distance for **11′**-6,6 of 1.85 Å was taken from the X-ray structural study of $(\eta^6\text{-}1,3,5\text{-}C_6H_3Me_3)_2Nb$ [30]. The rotational barrier for the $(HO)_3Nb$ groups was minimal (~ 0.1 eV), as expected for this cylindrically symmetric fragment, hence rotational conformers were ignored.

The **11′**-6,6 → **11′**-3,3 transit was performed by calculating the interfragment interaction as d_1 was varied from 0.0 to 1.4 Å in increments of 0.1 Å, while the **11′**-6,6 → **11′**-2,2 transit involved varying d_2 from 0.0 to 1.2 Å in 0.1 Å increments. Fig. 4 illustrates plots of the two transits, and reveals a somewhat surprising result. Although the interfragment energies of **11′**-3,3 and **11′**-2,2 are >12 eV more favorable than **11′**-6,6, they cannot be distinguished. As a consequence, even though the $\mu{:}\eta^2,\eta^2$-configurations generated by crystallographic models of the niobium and tantalum complexes are certainly plausible, some ambiguity with respect to a stable $\mu{:}\eta^3,\eta^3$-alternative clearly persists.

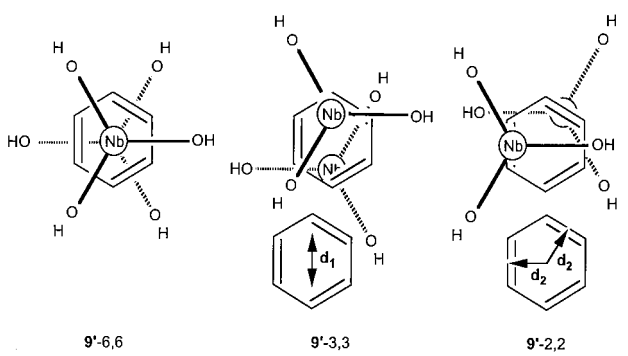

Fig. 3. Geometries of the $\mu{:}\eta^6,\eta^6$-(**11′**-6,6), $\mu{:}\eta^3,\eta^3$-(**11′**-3,3), and $\{(HO)_3Nb\}_2(\mu{:}\eta^2,\eta^2\text{-}C_6H_6)$ (**11′**-2,2) models used in the EHMO interfragment energetics analysis; d_1 and d_2 indicate the transit parameters from **11′**-6,6 to **11′**-3,3 and **11′**-2,2.

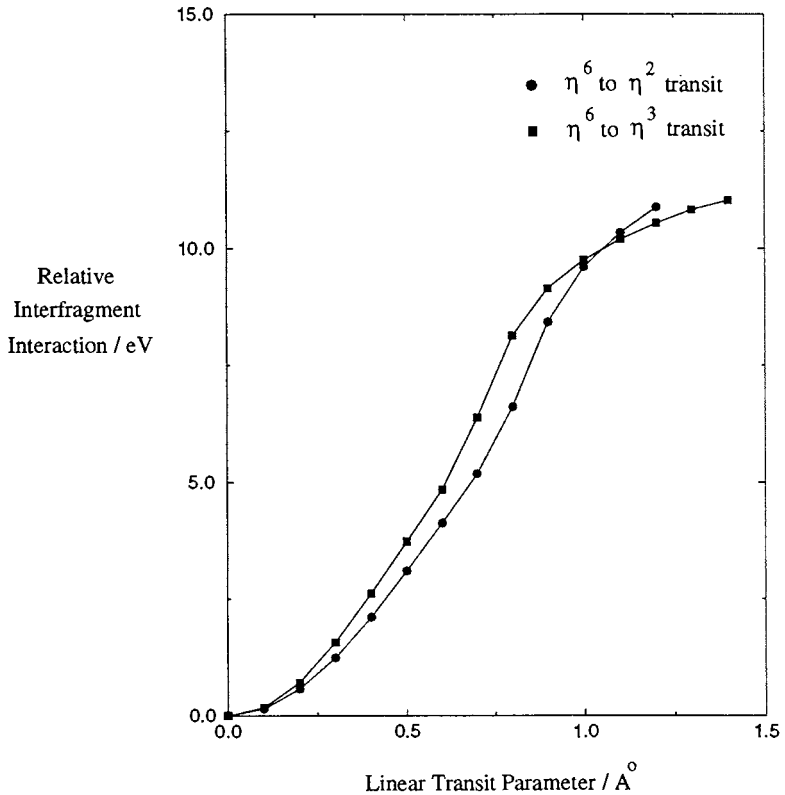

Fig. 4. Relative interfragment interaction ($-\Delta E$, eV) as a function of linear transit parameter (Å) for **11**′-6,6→**11**′-3,3 and **11**′-6,6→**11**′-2,2. The stronger the interaction, the more positive the value.

3. Summary

$(Silox)_3Nb(\eta^2\text{-}N,C\text{-}4\text{-}NC_5H_4CH_3)$ (**6**) is a functional equivalent of '$(silox)_3Nb$' according to olefin adduct formation and O-atom abstraction reactions. One adduct, $\{(silox)_3Nb\}_2(\mu{:}\eta^2,\eta^2\text{-}C_6H_6)$ (**11**), was examined structurally and via calculations. Its distorted $\mu{:}\eta^2,\eta^2$-arene binding mode is reminiscent of its tantalum analogue, yet no energetic difference between it and an alternate conformer containing an $\mu{:}\eta^3,\eta^3$-benzene was discerned via calculations.

4. Experimental

4.1. General considerations

All manipulations were performed using either glovebox or high-vacuum techniques. Hydrocarbon and ethereal solvents were dried over and vacuum transferred from sodium benzophenone ketyl (with 3–4 ml tetraglyme/l added to hydrocarbons). Benzene-d_6 was sequentially dried over sodium and 4 Å molecular sieves, then stored over and vacuum transferred from sodium benzophenone ketyl. Cyclohexane-d_{12} was dried over sodium, then stored over and vacuum transferred from Na/K alloy. All glassware was base-washed and oven dried. NMR tubes for sealed tube experiments were flame dried under dynamic vacuum immediately prior to the experiment. $(silox)_3MCl_2$ (M = Nb, **1**; Ta, **2**) [31] and $(silox)_3Nb(\eta^2\text{-}N,C\text{-py})$ (**5**) [21] were prepared according to literature procedures. Ethylene, ethylene oxide, N_2O, NO (Matheson) and styrene (Aldrich) were used as received; 4-picoline (Aldrich) was distilled and stored over 4 Å sieves.

^1H- and $^{13}C\{^1H\}$-NMR spectra were obtained using Varian XL-200, XL-400, VXR-400S, and Unity-500 spectrometers. IR spectra were recorded on a Nicolet Impact 410 spectrometer interfaced to a Gateway 2000 computer. Combustion analyses were performed by Oneida Research Services, Whitesboro, NY, or Robertson Microlit Laboratories, Madison, NJ. Cyclic voltammetry was performed on a Bioanalytical Systems (BAS) CV-27 Cyclic Voltammograph coupled to a BAS RXY Recorder. The molecular weight of **3** was determined using benzene cryoscopy on a home-built device.

4.2. Procedures

4.2.1. $[^nBu_4N][(silox)_3MCl_2]$ (M = Nb, $[^nBu_4N]$**1**; Ta, $[^nBu_4N]$**2**)

To a flask containing $(silox)_3TaCl_2$ (**2**) (500 mg, 0.555 mmol), anhydrous $^nBu_4NCl$ (154 mg, 0.555 mmol) and 0.9% Na/Hg (1.61 g Na, 0.61 mmol) was distilled 20 ml

THF at −78°C. A green color developed as the solution was warmed to 25°C and stirred for 1 h. After stirring for 12 h, the solution was filtered through Celite and concentrated to 10 ml. Hexanes (40 ml) were added and the solution was stirred for 30 min at 25°C, yielding 510 mg (81%) blue–green crystals of [^{n}Bu$_4$N]**2**, which were collected by filtration. Slow clouding of the crystals was observed after several days. ^{1}H-NMR (THF-d_8) spectroscopy revealed a broad singlet at δ 1.83 (^{t}Bu) in addition to ^{n}Bu signals, and traces of **2**, (silox)$_3$Ta, and other unidentified impurities. The same procedure was followed for [^{n}Bu$_4$N]**1**, yielding a blue–green substance with questionable crystallinity. Its ^{1}H-NMR (THF-d_8) spectrum exhibited a broad singlet at δ 1.78 (^{t}Bu) in addition to ^{n}Bu signals, and traces of **3** and other unidentified impurities.

*4.2.2. (Silox)$_3$NbCl (**3**)*

To a 50 ml flask attached to a 180° needle valve were added 2.053 g (silox)$_3$NbCl$_2$ (**1**, 2.534 mmol), 1.05 equivalents of Na (7.02 g) as 0.9% Na/Hg, and 30 ml THF at −78°C. The solution was allowed to warm to 25°C and stirred for 3 h, as the color changed to deep green, indicative of [Na(THF)$_x$][(silox)$_3$NbCl$_2$] ([Na(THF)$_x$]**1**). The solvent was removed and the residual was left under vacuum for 12 h, during which time the blue–green powder turned purple–gray. The residual Hg was decanted off and 15 ml hexanes were added. The purple solution was filtered, the salt cake washed three times with 5 ml hexanes, and the solution was concentrated to 10 ml. Filtration at −78°C afforded purple microcrystals. A second crop was collected for a total of 1.485 g **3** (76% yield). ^{1}H-NMR (C_6D_6): δ 1.67 (br s, ^{t}Bu); ^{13}C{^{1}H}-NMR (C_6D_6): δ 50.4 (C(*C*H$_3$)$_3$), 73.2 (Si*C*Me$_3$). Anal. Calc. for $C_{36}H_{81}Si_3O_3NbCl$: C, 55.82; H, 10.54. Found: C, 55.28; H, 10.52%. M_w Calc.: 775. Found: 754. Evan's method: 1.65 μ_B.

*4.2.3. (Silox)$_3$ClNb(py) (**3**-py)*

To a flask containing 45 mg **3** (0.058 mmol) was transferred 4 ml pyridine at −78°C. An ink-blue color appeared as the pyridine melted and warmed to 25°C. The solution was stirred for 20 min, the volatiles were removed and the residual was triturated with three 5 ml portions of hexanes and dried to yield a blue powder. ^{1}H-NMR (C_6D_6): δ −13.16 (s, 2H, *o*-H of py), −12.95 (s, 1H, *p*-H of py), 1.92 (br s, 81H, ^{t}Bu), 12.79 (s, 2H, *m*-H of py). Since **3** was also detected, **3**-py was not subjected to further analysis.

*4.2.4. (Silox)$_3$Nb(η^2-N,C-4-NC$_5$H$_4$CH$_3$) (**6**)*

To a 50 ml flask containing 500 mg (0.617 mmol) (silox)$_3$NbCl$_2$ (**1**) and 2.1 equivalents 0.9% sodium amalgam (30 mg Na in 3.3 g Hg) at −78°C was distilled 3 ml 4-picoline and 25 ml Et$_2$O. Upon slowly warming to 25°C, the solution was stirred for 10 h and the solvent removed. The solid was triturated twice with 4 ml hexanes, the amalgam was decanted away, and the remaining material was dissolved in 20 ml hexanes and filtered. The residue was washed three times with hexanes and the solvent was removed. The solid was dissolved in 2 ml Et$_2$O, cooled to −78°C, and filtered to afford 215 mg (42%) dark brown microcrystals. ^{1}H-NMR (toluene-d_8, −50°C): δ 1.25 (s, 81H, ^{t}Bu), 1.91 (s, 3H, Me), 4.33 (s, 1H, NbC^{2}H), 5.27 (d, 1H, C^{5}H, $J_{5,6}$ = 6.4 Hz), 6.63 (s, 1H, C^{3}H), 7.75 (d, 1H, C^{6}H, $J_{5,6}$ = 6.4 Hz); ^{13}C{^{1}H}-NMR (toluene-d_8, −50°C) δ 23.41 (C(*C*H$_3$)$_3$), 29.50 (CH$_3$), 30.46 (SiC), 91.31 (C^{2}H), 110.00 (C^{5}H), 147.30 (C^{6}H), C^{3}H and C^{4}Me not located due to overlap with solvent. Anal. Calc. for $C_{42}H_{88}NSi_3O_3Nb$: C, 60.61; H, 10.66; N, 1.68. Found: C, 60.74; H, 10.78; N, 1.46%.

*4.2.5. (Silox)$_3$Nb(η^2-H$_2$CCHPh) (**8**)*

To a 25 ml round-bottom flask containing 567 mg (0.693 mmol) (silox)$_3$Nb(η^2-N,C-py) (**5**) and 18 ml cyclohexane at −78°C was syringed 0.5 ml styrene. Upon warming to 25°C, the solution was stirred for 6 h, and the solvent was removed. Green–brown **5** was crystallized from pentanes at −78°C (254 mg, 44%). ^{1}H-NMR (C_6D_6): δ 1.19 (s, 81H, ^{t}Bu), 2.73 (dd, 1H, C*H*H, J = 10.6, 13.6 Hz), 3.03 (dd, 1H, CH*H*, J = 10.6, 14.7 Hz), 3.71 (dd, 1H, CHPh, J = 13.6, 14.7 Hz), 6.89 (t, 1H, *p*-H), 7.19 (d, 2H, *o*-H), 7.3 (d, 2H, *m*-H); ^{13}C{^{1}H}-NMR (C_6D_6): δ 23.9 (C(*C*H$_3$)$_3$), 31.1 (SiC), 73.2 (CH$_2$), 76.3 (CHPh), 124.7, 125.7, 129.1, 149.1 (Ph). Anal. Calc. for $C_{44}H_{89}Si_3O_3Nb$: C, 62.66; H, 10.64. Found: C, 61.93; H, 10.51%.

*4.2.6. (Silox)$_3$Nb=O (**9**)*

To a 10 ml flask containing 100 mg (silox)$_3$Nb(η^2-(N,C)-4-NC$_5$H$_4$CH$_3$) (**6**) (0.12 mmol) was distilled 5 ml of benzene at 77 K. N_2O (118 Torr, 1.1 equivalents) was condensed at 77 K from a calibrated gas bulb (20.8 ml). Upon thawing the dark brown solution turned to a tan color and stirring was continued overnight. The benzene was stripped to give **9** as a tan powder (48 mg, 53% yield). ^{1}H-NMR (C_6D_6): δ 1.27; ^{13}C{^{1}H}-NMR (C_6D_6): δ 30.96 (C(*C*H$_3$)$_3$), 24.06 (SiC). IR (Nujol) ν(Nb=O) = 884 cm^{-1} (tentative). Anal. Calc. for $C_{36}H_{81}O_4Si_3Nb$: C, 57.26; H, 10.80. Found: C, 57.28; H, 10.68%.

*4.2.7. {(Silox)$_3$Nb}$_2$(μ:η^2,η^2-C$_6$H$_6$) (**11**)*

To a 10 ml flask containing 89 mg (silox)$_3$Nb(η^2-(N,C)-4-NC$_5$H$_4$CH$_3$) (**6**) (0.11 mmol) and 97 mg (silox)$_3$Ta (**4**) (0.12 mmol, 1.1 equivalents) was distilled benzene (8 ml) at 77 K. When the benzene thawed a brown solution was observed. After 2 h a purple–red precipitate was observed and the benzene was stripped. The resulting dark solid was triturated twice with pentane (8 ml). An additional 8 ml of pentane was added and the resulting slurry filtered. The filtered material was washed twice with pentane (2 ml) to give dark

brown **11** (45 mg, 54% yield). IR (Nujol) 889 cm^{-1}, 834 cm^{-1}, 811 cm^{-1}. Anal. Calc. for $C_{78}H_{168}O_6Si_6Nb_2$: C, 60.43; H, 10.92. Found: C, 59.95; H, 10.63.

4.2.8. NMR tube-scale reactions

*4.2.8.1. **6** and N_2O.* An NMR tube attached to a 14/20 joint was charged with 20 mg $(silox)_3Nb(\eta^2\text{-}(N,C)\text{-}4\text{-}NC_5H_4CH_3)$ (**6**) (0.024 mmol) and ~0.6 ml C_6D_6. The solution was degassed three times and N_2O condensed (36 Torr, 0.025 mmol, 1.05 equivalents) at 77 K from a calibrated gas bulb (13.0 ml). When the benzene thawed, gas evolution and immediate discharge of the dark brown color was observed. ^{1}H- and $^{13}C\{^1H\}$-NMR showed complete conversion to $(silox)_3Nb{=}O$ (**9**) and 4-picoline (δ 1.76 s, δ 6.56 d, and δ 8.47 d)

*4.2.8.2. **6** and NO.* An NMR tube attached to a 14/20 joint was charged with 18 mg **6** (0.021 mmol) and ~0.6 ml C_6D_6. The solution was degassed three times and NO condensed, 32 Torr (0.023 mmol, 1.05 equivalents) at 77 K from a calibrated gas bulb (13.0 ml). When the benzene thawed an immediate discharge of the dark brown color was observed to give a bright yellow solution. The ^{1}H-NMR spectrum indicated the presence of **9** and 4-picoline.

*4.2.8.3. **6** and ethylene oxide.* To an NMR tube containing 19 mg **6** (0.023 mmol) and ~0.6 ml C_6D_6 was condensed 22.2 Torr of ethylene oxide (0.025 mmol, 1.1 equivalents) at 77 K from a calibrated gas bulb (20.8 ml). After 3 days at 25°C the reaction was complete. A ^{1}H-NMR spectrum showed a ~1.5:1 ratio of **9** (δ 1.27) and $(silox)_3Nb(\eta^2\text{-}H_2CCH_2)$ (**7**) along with free ethylene (δ 5.26), unreacted ethylene oxide (δ 2.11) and 4-picoline.

*4.2.8.4. $(Silox)_3Nb(\eta^2\text{-}H_2CCH_2)$ (**7**) from **4** and CH_2CH_2.* An NMR tube attached to a ground glass joint was charged with **5** (0.015 g, 0.018 mmol) in 0.6 ml C_6D_6 and attached to a 24.4 ml gas bulb. Ethylene (138 Torr, 0.181 mmol) of was admitted via the gas bulb, and the tube was sealed. The solution quickly bleached to light orange, and ^{1}H-NMR spectroscopy revealed complete conversion to **7**. ^{1}H-NMR δ 1.21 (s, 81H, ^{t}Bu), 2.40 (br s, 4H, C_2H_4).

*4.2.8.5. $(Silox)_3Ta$ (**4**) and N_2O.* An NMR tube attached to a 14/20 joint was charged with 24 mg $(silox)_3Ta$ (**4**) (0.029 mmol) and ~0.4 ml C_6D_6. The solution was degassed three times and N_2O condensed (28 Torr, 0.029 mmol, 1.0 equivalents) at 77 K from a calibrated gas bulb (19.6 ml). When the benzene thawed, gas evolution and immediate discharge of the blue color was observed. ^{1}H-NMR analysis showed complete conversion to $(silox)_3Ta{=}O$ (**10**) (δ 1.27 s).

*4.2.8.6. **4** and NO.* An NMR tube attached to a 14/20 joint was charged with 22 mg **4** (0.027 mmol) and ~0.4 ml C_6D_6. The solution was degassed three times and NO condensed (14 Torr, 0.014 mmol, 0.53 equivalents) at 77 K from a calibrated gas bulb (19.6 ml). When the benzene thawed a fading of the blue color was observed, and the ^{1}H-NMR spectrum indicated the presence of **10** and **4** in a 1:1 ratio.

*4.2.9. Cyclic voltammetry of **1** and **2***

A silver wire reference electrode, a platinum wire counterelectrode, and a platinum working electrode (0.0096 cm^2) were employed. Dichlorides **1** and **2** were examined under the following conditions: THF, [analyte] = 0.001 M, $[^nBu_4NPF_6] = 0.1$ M.

*4.2.10. Single-crystal X-ray diffraction study of $\{(silox)_3Nb\}_2(\mu{:}\eta^2,\eta^2\text{-}C_6H_6)\cdot C_6H_6$ (**11**$\cdot C_6H_6$)*

In the dry-box a solution of $(silox)_3Ta$ (**4**) (45 mg in 2 ml of benzene) was added to a solution of $(silox)_3Nb(\eta^2\text{-}(N,C)\text{-}4\text{-}NC_5H_4CH_3)$ (**6**) (50 mg in 5 ml of benzene) in a small vial. The contents of the vial were shaken vigorously for 1 min and then left alone. After 5 h, single crystals of **11**$\cdot C_6H_6$ were observed. A purple–red crystal $0.3 \times 0.2 \times 0.02$ mm was placed under a coating of polyisobutylene at 173 K. The data were collected on a Bruker diffractometer (graphite monochromated Mo–K_α radiation, $\lambda = 0.71073$ Å) equipped with a SMART 1K CCD detector. Systematic absences were consistent with the triclinic space group, $P\bar{1}$. Overall, 14 034 reflections were measured (0.3° ω scan), and 10 041 of them were independent (R_{int} = 0.0354). An empirical correction for absorption (SADABS) was applied to the data. The structure was solved by direct methods (SHELX). All non-hydrogen atoms were anisotropically refined and hydrogen atoms were treated as idealized contributions; a benzene solvent molecule was suitably modeled. The largest difference peak (1.440 e $Å^{-3}$) and hole (-1.511 e $Å^{-3}$) were a consequence of the disorder. Various disorder models were applied to the benzene bridge, and the half-occupency $\mu{:}\eta^2,\eta^2\text{-}C_6H_6$ configuration proved superior. The geometry of the benzene was unreasonable, so the carbon–carbon distances were restrained (1.40 Å) and the ring was restrained to be flat using options available within SHELX.

4.2.11. EHMO calculations

Extended Hückel molecular orbital calculations were conducted using the YAEHMOP package [28].

5. Supplementary material

Data for $\{(silox)_3Nb\}_2(\mu{:}\eta^2,\eta^2\text{-}C_6H_6)\cdot C_6H_6$ (**11**$\cdot C_6H_6$) have been deposited at the Cambridge Crys-

tallographic Data Centre (CCDC 128546). Copies of this information may be obtained free of charge from The Director, CCDC, 12 Union Road, Cambridge, CB2 1EZ, UK (Fax: +44-1223-336-033; e-mail: deposit@ccdc.cam.ac.uk or www: http://www.ccdc.cam.ac.uk).

Acknowledgements

We thank the National Science Foundation and Cornell University for support of this research.

References

[1] C.C. Cummins, Prog. Inorg. Chem. 47 (1998) 685.
[2] C.E. Laplaza, M.J.A. Johnson, J.C. Peters, A.L. Odom, E. Kim, C.C. Cummins, G.N. George, I.J. Pickering, J. Am. Chem. Soc. 118 (1996) 8623.
[3] C.E. Laplaza, A.L. Odom, W.M. Davis, C.C. Cummins, J.D. Protasiewicz, J. Am. Chem. Soc. 117 (1995) 4999.
[4] A.L. Odom, C.C. Cummins, J.D. Protasiewicz, J. Am. Chem. Soc. 117 (1995) 4999.
[5] M. Vivanco, J. Ruiz, C. Floriani, A. Chiesi-Villa, C. Rizzoli, Organometallics 12 (1993) 1802.
[6] S.L. Latesky, J. Keddington, A.K. McMullen, I.P. Rothwell, J.C. Huffman, Inorg. Chem. 24 (1985) 995.
[7] K.J. Covert, A.-R. Mayol, P.T. Wolczanski, Inorg. Chim. Acta 263 (1997) 263.
[8] K.J. Covert, P.T. Wolczanski, S.A. Hill, P.J. Krusic, Inorg. Chem. 31 (1992) 66.
[9] C.C. Cummins, C.P. Schaller, G.D. Van Duyne, P.T. Wolczanski, E.A.-W. Chan, R. Hoffmann, J. Am. Chem. Soc. 113 (1991) 2985.
[10] C.P. Schaller, C.C. Cummins, P.T. Wolczanski, J. Am. Chem. Soc. 118 (1996) 591.
[11] J. de With, A.D. Horton, Angew. Chem. Int. Ed. Engl. 32 (1993) 903.
[12] C.P. Schaller, P.T. Wolczanski, Inorg. Chem. 32 (1993) 131.
[13] D.F. Schafer II, P.T. Wolczanski, J. Am. Chem. Soc. 120 (1998) 4881.
[14] J.L. Bennett, P.T. Wolczanski, J. Am. Chem. Soc. 119 (1997) 10696.
[15] P.T. Wolczanski, Polyhedron 14 (1995) 3335.
[16] D.R. Neithamer, R.E. LaPointe, R.A. Wheeler, D.S. Richeson, G.D. Van Duyne, P.T. Wolczanski, J. Am. Chem. Soc. 111 (1989) 9056.
[17] J.B. Bonanno, P.T. Wolczanski, E.B. Lobkovsky, J. Am. Chem. Soc. 116 (1994) 11159.
[18] J.B. Bonanno, T.P. Henry, D.R. Neithamer, P.T. Wolczanski, E.B. Lobkovsky, J. Am. Chem. Soc. 118 (1996) 5132.
[19] D.R. Neithamer, L. Párkányi, J.F. Mitchell, P.T. Wolczanski, J. Am. Chem. Soc. 110 (1988) 4421.
[20] K.J. Covert, D.R. Neithamer, M.C. Zonnevylle, R.E. LaPointe, C.P. Schaller, P.T. Wolczanski, Inorg. Chem. 30 (1991) 2494 and references therein.
[21] T.S. Kleckley, J.L. Bennett, P.T. Wolczanski, E.B. Lobkovsky, J. Am. Chem. Soc. 119 (1997) 247.
[22] (a) T.S. Kleckley, Ph.D. Thesis, Cornell University, 1998. (b) T.S. Kleckley, P.T. Wolczanski, E.B. Lobkovsky, manuscript in preparation.
[23] S.D. Gray, K.J. Weller, M.A. Bruck, P.M. Briggs, D.E. Wigley, J. Am. Chem. Soc. 117 (1995) 10678 and references therein.
[24] UV–vis spectral features are similar to those of structurally characterized tungsten and rhenium tbp derivatives, $(silox)_3MCl_2$ (M = W, Re). (a) R.E. Douthwaite, P.T. Wolczanski, E.B. Lobkovsky, unpublished results. (b) R.E. Douthwaite, P.T. Wolczanski, E. Merschrod, Chem. Commun. (Cambridge) (1998) 2591.
[25] (a) G. Parkin, J.E. Bercaw, J. Am. Chem. Soc. 111 (1989) 391. (b) A. van Asselt, B.J. Burger, V.C. Gibson, J.E. Bercaw, J. Am. Chem. Soc. 108 (1986) 5347.
[26] (a) J.M. Casas, J. Forniés, F. Martínez, A.J. Rueda, M. Tomás, A.J. Welch, Inorg. Chem. 38 (1999) 1529. (b) R.M. Chin, L. Dong, S.B. Duckett, M.G. Partridge, W.D. Jones, R.N. Perutz, J. Am. Chem. Soc. 115 (1993) 7685. (c) C.-S. Li, C.-H. Cheng, F.-L. Liao, S.-L. Wang, J. Chem. Soc. Chem. Commun. (1991) 710. (d) K.-B. Shiu, C.-C. Chou, S.-L. Wang, S.-C. Wei, Organometallics 9 (1990) 286.
[27] (a) R.M. Chin, L. Dong, S.B. Duckett, W.D. Jones, Organometallics 11 (1992) 871. (b) W.D. Harman, H. Taube, J. Am. Chem. Soc. 109 (1987) 1883. (c) H. van der Heijden, A.G. Orpen, P. Pasman, J. Chem. Soc. Chem. Commun. (1985) 1576.
[28] (a) The YAEHMOP extended Hückel molecular orbital package is freely available on the WWW at http://overlap.chem.cornell.edu:8080/yaehmop.html. (b) G.A. Landrum, W.V. Glassey, bind (ver 3.0). bind is distributed as part of (a).
[29] D.R. Lide (Ed.), CRC Handbook of Chemistry and Physics, CRC Press, New York, 1998, pp. 9–25.
[30] F. Calderazzo, F. Gingl, G. Pampaloni, L. Rocchi, J. Strähle, Chem. Ber. 125 (1992) 1005.
[31] R.E. LaPointe, P.T. Wolczanski, G.E. Van Duyne, Organometallics 4 (1985) 1810.